4th San Miniato Topical Seminar

EXPERIMENTAL APPARATUS FOR HIGH ENERGY PARTICLE PHYSICS AND ASTROPHYSICS

San Miniato, Tuscany, Italy   28 May – 1 June 1990

Editors
P. Giusti and F.-L. Navarria
Dipartimento di Fisica e INFN
Università di Bologna

P.G. Pelfer
Dipartimento di Fisica e INFN
Università di Firenze

DEVELOPMENT OF SPARK COUNTERS
FOR PARTICLE IDENTIFICATION

Yu.N.Pestov

Institute of Nuclear Physics, Novosibirsk 90, 630090, USSR

ABSTRACT

The status of the R&D programme of the TOF system based on spark counters for particle identification is described. The main parameters of this system are: the spark counter time resolution is σ_t=25ps, the material thickness is 0.1 radiation length, the geometrical thickness is 100 mm. A spark counter prototype for the TOF system has been constructed. Its performance proves the feasibility of the TOF system with the designed parameters.

1. Introduction

The idea of a spark counter with a localized discharge was proposed and realized at INP, Novosibirsk in 1971[1]. The first application of these spark counters in an experiment was in the pion form factor measurement near the threshold at the VEPP2 collider in 1978-1981 [2]. In that work the spark counters were used both for particle identification by TOF and, for determination of the geometrical characteristics of the events.

During the last ten years the R&D programme of spark counters at INP, Novosibirsk and at some other world laboratories was aimed at better understanding of the physical processes in the spark counter in order to improve their characteristics: the life time, the time and coordinate resolution, the thickness in term of traversed matter, the technological design simplicity, etc. [3].

As a result of these efforts a TOF system was proposed based on spark counters [4]. The main parameters of this system are given in the second part of this report. In the third part the design of the spark counter prototype for this system is described. The performance of the prototype is given in the fourth part. In the last part of the report the conclusion is drawn about the feasibility of the TOF system with the project parameters.

2. Project of the TOF system

The TOF system consists of two layers of spark counters (Fig. 1). Each spark counter has electrodes 40 mm wide, 2 mm thick and several metres total length. The spark counter container is a tube with a diameter of 50 mm, so the thickness of the layers is equal to 100 mm. The average material thickness for particles crossing the system normally to the layers is equal to 0.1 radiation length. Over a flight path of 1m the time resolution for each counter of σ_t=25 ps allows one to distinguish pions and kaons up to the momentum of 2.7 GeV/c, kaons and protons up to 4.6 GeV/c at the 2σ level.

3. Design and principal electric scheme of the spark counter prototype for the TOF system

3.1. Prototype construction

Fig. 2 shows the principle of the construction of the spark counter prototype. It consisted of two spark counter electrodes (1), a plexiglass electrode support (2) and a container (3).

Spark counter electrodes were 2 mm thick and 40 mm wide. The anode electrode was made of semiconductive glass with a bulk resistivity $\rho=6\cdot10^9$ Ohm·cm. On the outside to the gas gap of the anode electrode the copper layer was deposited by the magnetron cathode sputtering [5]. Sparks induced electric signals on this conductive layer used for the readout. The cathode was made of usual glass, on which the copper layer was deposited by the magnetron cathode sputtering. Electrode surfaces were polished with a tolerance of 1 μm on any electrode region of the order of 40x40 mm. The electrode material thickness averaged over the container size was equal to 0.029 radiation length.

The gas gap of 0.1 mm was produced by two lines of pins glued in the semiconductive electrode. The number of pins formed 40 pieces on each 0.5 m counter length. The accuracy of their height with respect to the electrode surface was 0.5 μm. Around each pin the electric field decrease was formed by a smooth hollow in the semiconductive electrode. The dead area due to the decreased electric field around pins was less than 1.4% of an electrode area.

It was proposed that the spark counter total length would be made from separate spark counters put in the series on one plexiglass support. To check the connection between counters the prototype of the total length of 0.5 m was made of two spark counters with lengths of 0.2 m and 0.3 m.

The plexiglass hollow support for counter electrodes (Fig. 2,2) with the wall thickness of 1 mm was used also as a part of the gas flowthrough system. This system was designed to provide a

circular gas velocity in the gap of 1 m/s. The gas, coming from the circulation pump to the space over electrodes was directed through a gas filter to the gap and then through special holes into the plexiglass support, which was also connected the circulation pump. An intensive gas flow was required to provide spark counter long-term operation.

An aluminium tube with the inner diameter of 50 mm and the wall thickness of 5 mm was used in the prototype as a container of the counter (Fig. 2, 3). In the final design it was proposed to use as a container an aluminium tube with the wall thickness of 0.5 mm, corresponding to the averaged material thickness of 0.018 radiation length. This tube was pressurized successfully up to 25 atm. The working gas pressure is 11 atm.

Thus the total material thickness of a spark counter would be less than 0.05 radiation length.

3.2. Prototype electric scheme

Fig. 3 shows the electric scheme of the spark counter prototype. To simplify a signal external connection, a high positive voltage was applied to the spark counter anode. Electric signals from sparks travel to both ends of the counter in the strip line, formed by the conductive layers on the anode and the cathode. The measured impedance of this strip line was about 8 Ohm. As stated above, the prototype consisted of two spark counters, put close to one another on one plexiglass support. The signal strip lines of these spark counters were connected in series. The external connection to the strip was carried out through an insulation mylar film with the thickness of 0.1mm because of the high voltage was applied to the strip (Fig. 3, 2). A cable transformer was used to match the 8 Ohm signal cable (Fig. 3, 3).

4. Performance of the prototype

The gas mixture pressure of 12 atm was chosen to satisfy the condition that the efficiency of the spark counter with respect to charged particles should exceed 96%. One of the conditions required for the discharge localization in the spark counter is absorption of photons, produced by spark in a gas in the wide range of wavelenghts. Gas mixtures based on dyvinil (D), ethylene (Eth), isobutane (Is) and argon (Ar) provide absorption of photons with wavelengths under 220 nm. Special research has showed, that the best time resolution was obtained for the gas mixture of 0.3 atm D +0.3 atm Eth+2.4 atm Is+Ar [6]. A decrease in the dyvinil partial pressure down to 0.07 atm gave an increase of the spark counter time resolution [6].

The undermentioned spark counter prototype characteristics were obtained with these two gas mixtures, n.1 and n.2 accordingly. The threshold of charged particle detection was 3.13 kV for the

n.1 gas mixture and 2.9 kV for the n.2. The prototype characteristics were measured after detection of ~10^6 sparks/cm^2 to preliminary stabilize in time counter parameters.

4.1. Plateau curve and pulse height characteristics

Fig. 4 shows the plateau curves of the spark counter prototype obtained with a γ-source for two gas mixtures above. The counting rate increase quickly with overvoltage transforming into the Geiger discharge. For the first gas mixture the plateau is wider, than for the second one.

The dependence of the average discharge area on the overvoltage is shown in Fig. 5. For the second gas mixture discharge localization was visibly worse, than for the first one, because there was not enough of dyvinil for photon absorption.

The signal rise time from the prototype was expected to be fractions of nanosecond. As a load of 50 Ohm on the oscillograph with its own rise time of 2 ns, a pulse height ranged from 0.2- 0.4 V at the plateau end. A pulse had an exponential tail with the decay time of about 5 ns. Fig. 6 show the spectrum of the charge distribution from the prototype at the plateau end. The FWHM of this distribution is equal approximately to the mean pulse height.

4.2. Time resolution

The timing properties of the prototype were studied in the experiment, shown schematically in Fig. 7. The time of flight for cosmic particles was measured between the prototype and a spark counter with an electrode thickness of 5 mm and an area 100x100 mm^2. Both counters were filled with the same gas mixture and the measurements were performed at the same overvoltages. Events, that has signals from both counters simultaneously, were used for the trigger. The firing of the scintillation counter, placed behind a 40 cm lead shield, was logged by a bit in the computer. In the present geometry of the experiment the marked events covered a large portion of the length of the prototype. Fig. 8 shows the event distribution along the prototype. Near the connection place of two spark counters in the prototype there is a «dead» region, which failed to detect particles. The size of this «dead» region along the prototype, obtained from Fig. 8, is 2-3 mm or about 0.5% of the 0.5 m prototype length.

Fig. 9 shows the dependence of the prototype time resolution on the overvoltage for the two gas mixtures above. It was therefore assumed that the prototype and the 100x100 mm^2 area spark counter had similar time resolutions. This assumption is proved by the fact, that the results obtained coincide within the measurement accuracy with the time resolution of the 100x100 mm^2 area spark counter, measured in a previous work [6].

The best time resolution obtained in this experiment was σ_t=27 ps.

4.3. Rate capability

A detailed study of the rate capability of the prototype was not carried. The maximum counting rate of a spark counter F_{max} is determined by an average discharge area S and a high voltage recovery time T : $F_{max}=1/SxT$. With an average discharge are $S=1$ mm^2 and with the prototype recovery time $T=0.01$ s, F_{max} is equal to 10 kHz/cm^2. It was shown that the semiconductive electrode resistivity of a spark counter could be decreased 6 times, which would provide the maximum counting rate $F_{max}=60$ kHz/cm^2. The counter time resolution degrades with a counting rate increase. From the experiments with the spark counters with electrode thickness of 5 mm it can be concluded, that the counting rate of 2 kHz/cm^2 would decrease the time resolution of the prototype by 15% [6].

4.4. Life time

The main reason for aging of the spark counter consists in polymerization of a gas media during the spark counter operation. It is possible to get expected estimation of the prototype life time from the experiments with the spark counters with the electrode thickness of 5 mm [6]. The prototype would detect at the overevoltage $U/U_o=2$ more than $4 \cdot 10^9$ particles/cm^2 with the first gas mixture and more than $2 \cdot 10^{10}$ particles/cm^2 with the second one.

It is necessary to make two important remarks.

1) To avoid background, spark counter electrodes must be carefully polished, cleaned and scratches must be excluded. This is especially important, when a spark counter operates with the first gas mixture.

2) A background counting rate produced by scratches or dust on the electrodes would decrease the spark counter life time considerably. It is necessary to carry out measurements of this background counting rate bahaviour over a long time interval.

4.5. Coordinate resolution and electronics

The particle coordinate along spark counter strips (Z-coordinate) is determined by the difference of the arrival times of the signals at opposite ends of the spark counter. In paper [6] the longitudinal coordinate resolution of 0.5 mm was obtained for the spark counter with an electrode thickness of 5 mm and it was determined by the electronic resolution. In paper [6] it was also shown, that the spark counter coordinate and time resolution remained constant within the measurement accuracy at an angle of cosmic-ray particles inclination to the electrode plane changing at least in range from 30 to 150 degrees.

The electronics in the present work was the same as in [6] and it consisted of discriminators with a low threshold of 6 mV and time-amplitude converters with there own resolution of 1-2 ps. Analog signals were digitized by a 13-bit amplitude-digital converter. The range of measurements was 20 ns at the resolution of 3 ps. To improve integral and differential nonlinearities up to 0.005% and 1.5% respectively, the electronics was calibrated by a random pulse generator. The sensitivity of a time scale of the electronics was estimated by the calibration using an air delay line.

Thus, the expected longitudinal coordinate resolution of the prototype would be about $\sigma_z=0.5$ mm. The transversal coordinate accuracy of the prototype is determined by the electrode width $\sigma_x= 40/\sqrt{12} =12$ mm.

Conclusion

The performance of the spark counter prototype considered above proves the feasibility of the TOF system with given parameters.

The spark counter time resolution $\sigma_t=25$ ps for a life time over $4 \cdot 10^9$ sparks/cm^2 seems to be real with the first gas mixture. A five times longer life time could be obtained for a time resolution $\sigma_t=40$ ps with the second gas mixture. The rate capability of the spark counter would exceed 2 kHz/cm^2. The longitudinal coordinate resolution of the spark counter $\sigma_z=0.5$ mm may provide useful additional information to coordinate measurements in drift chambers in real experiments. In this work the feasibility of lengthening the spark counter by connecting separate counters in series was demonstrated.

Two technological problems must be solved for the mass production of the spark counters for the TOF system. Firstly, a convenient technology for an electrode support production must be found. Secondly, it is necessary to find a simple technology for the precise glueing of pins, which make the gas gap, in a semiconductive electrode. The rest of the spark counter components look simple enough for the counter mass production.

References

1. V.V. Parchomchuck, Yu.N. Pestov and N.V. Petrovykh, *NIM 93* (1971) 269.

2. I.V. Vasserman, P.M. Ivanov, Yu.N. Pestov et al. *jadernaja Fisica* 28 (1978) 968; *Jadernaja fisica* 33 (1981) 709.

3. V.D. Laptev, Yu.N. Pestov and N.V. Petrovykh, *Prib. Tekh. Eksp.* 6 (1975) 36.

A.D. Afanas'ev, V.D. Laptev, Yu.N. Pestov and B.P. Sannikov, *Prib. Tekh. Eksp.* 6 (1975) 39.

Yu.N. Pestov and G.V. Fedotovich, *Preprint* INP-77-88, Novosibirsk (1977).

V.D. Laptev, Yu.N. Pestov et al. *Izv. AN SSSR*, 42 (1978) 1488.

Yu.N. Pestov, G.V. Fedotovich and K.N. Putilin, *Proc. Int. Conf. on Instrumentation of Colliding Beam Physics*, SLAC-250 UC-34D (1982) 127.

W.B. Atwood, G.B. Bowden, Yu.N. Pestov et al, *NIM* 206 (1983) 99.

Yu.N. Pestov, *Proc. Int. Conf. on Instrumentation of Colliding Beam Physics*, INF, Novosibirsk (1984) 163.

A. Ogawa, W.B. Atwood, N. Fujiwara, Yu.N. Pestov and R. Sugahara, *IEEE TRAS. NUCL. SCI.* NS-31 1 (1984) 121.

N. Fujiwara, A. Ogawa, Yu.N. Pestov and R. Sugahara, *NIM* A240 (1985) 275.

R. Cardarelli, R. Santonico, A. Di Biagio and A. Lucci, *NIM* A263 (1988) 20.

4. Yu.N. Pestov, *NIM* A265 (1988) 150.

5. Yu.N. Pestov, and K.N. Putilin, *Prib. Tekh. Eksp.* 6 (1988) 71.

6. Yu.N. Pestov, *Proc. Int. Conf. on Instrumentation of Colliding Beam Physics*, INP, Novosibirsk (1990) *in print*.
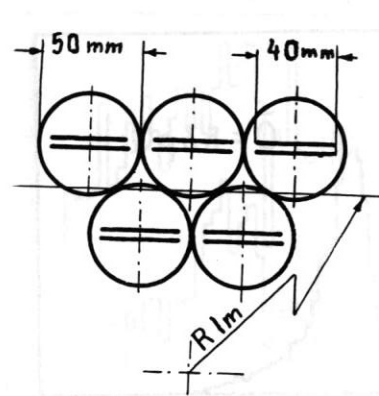
Fig. 1. A thin time-of-flight system based on spark counters.
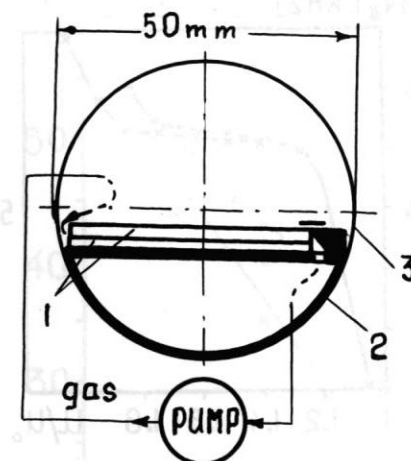
Fig. 2. Principal mechanical design of the prototype. 1-electrodes, 2-plexiglass support, 3-aluminium tube.
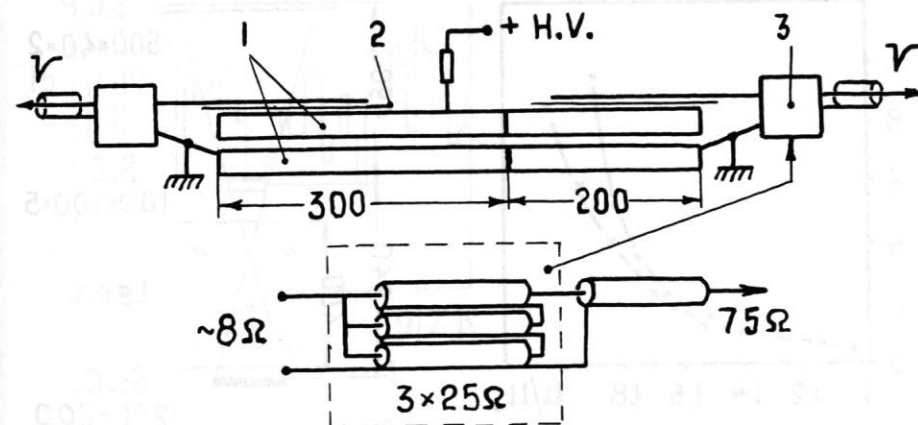
Fig. 3. Principal electrical design of the protype. 1-electrodes, 2-insulator, 3-transformer.
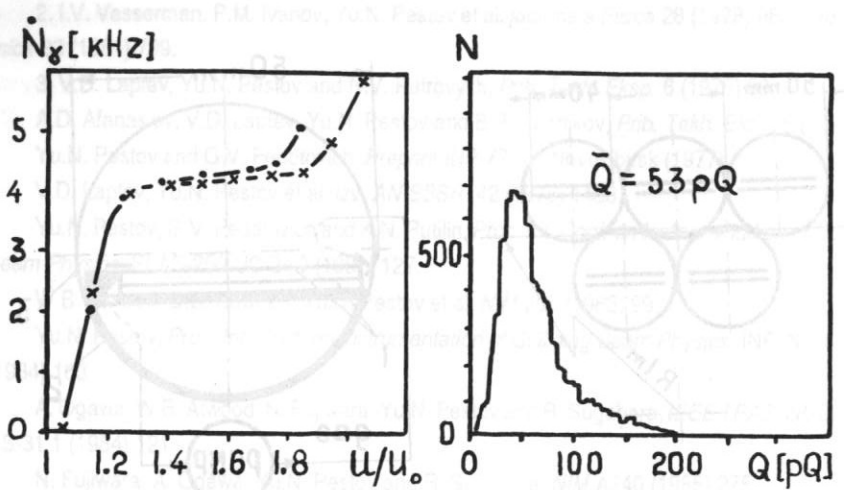
Fig. 4. Plateau curve of the prototype at two gas mixtures. x - N1, . -N2.
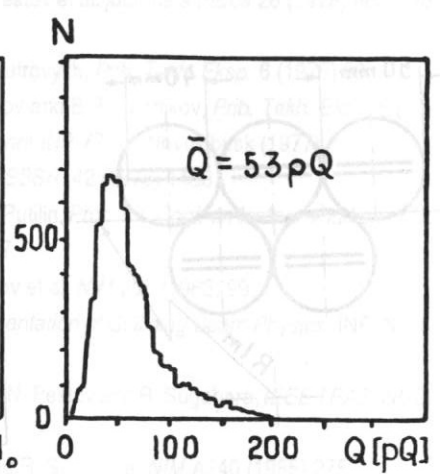
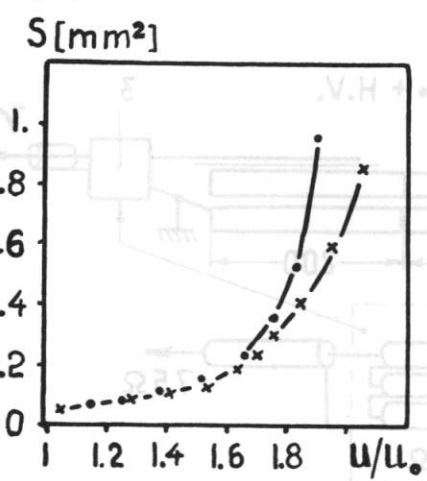Fig. 6. Pulse height distribution from the prototype at the N2 gas mixture, $U/U_0 = 1.83$.

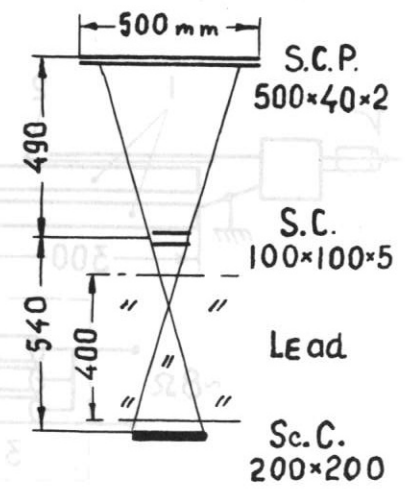Fig. 5. Dependences of average discharge area on overvoltage at two gas mixtures: x -N1, . -N2.
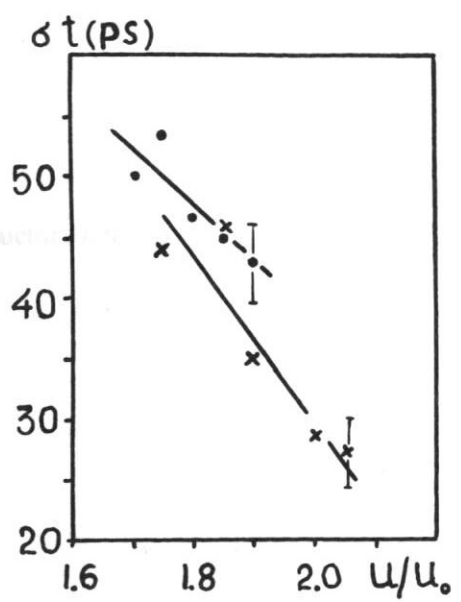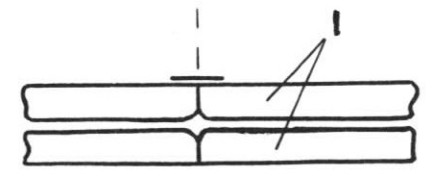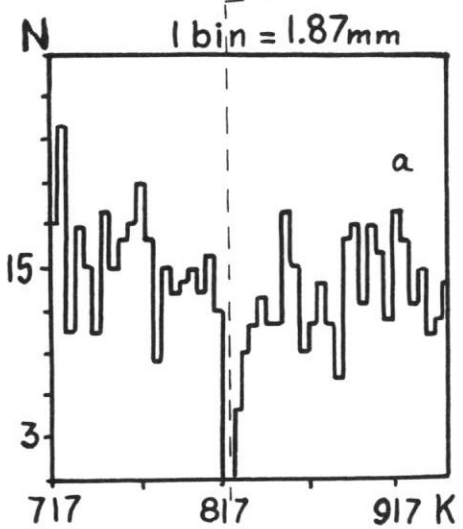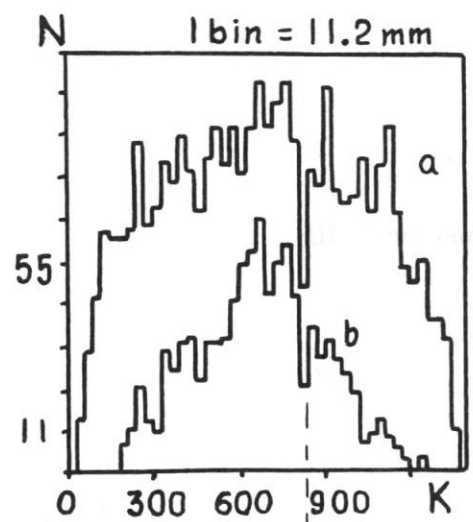

Fig. 7. Schematic drawing of the test setup.

Fig. 9. Prototype time resolution at two gas mixture_ x -N1, . -N2.

Fig. 8. Event distribution along the prototype: a-for simultaneous signals from two spark counters, b-for extra coincidence with scintillation counter signal. 1-counter electrodes.

ELECTROMAGNETIC CALORIMETER BASED ON LIQUID KRYPTON FOR THE KEDR DETECTOR

V.M.Aulchenko, A.E.Blinov, S.G.Klimenko, G.M.Kolachov,
L.A.Leontiev, A.P.Onuchin, V.S.Panin, S.G.Pivovarov,
Yu.V.Pril, V.A.Rodyakin, A.G.Shamov, Yu.I.Skovpen,
Yu.A.Tikhonov, V.A.Tayursky, V.I.Yurchenko
Institute of Nuclear Physics, Novosibirsk, USSR

M.Bazzotti, G.Lo Bianco, F.Lanni, F.Maggi, F.Palombo,
A.Sala
Dipartamento di Fisica dell'Universita' and Sezione IFN,
Milan, Italy

P.Frabetti, P.Cantoni, L.Stagni
Dipartamento di Fisica dell'Universita' and Sezione INFN,
Bolonia, Italy

P.F.Manfredi, D.Marioli, V.Re, V.Speziali
Dipartamento di Elettronica Universita' di Pavia and
Sezione INFN, Milan, Italy

Presented by A.P.Onuchin

Abstract

Effects, determining energy and spatial resolution of a calorimeter based on liquid krypton have been studied. At the prototype with 0.4ton of krypton the energy resolution is obtained 5.7% at 130MeV and 1.7% at 1200MeV. With strip width of 10mm the spatial resolutin is 0.4mm for cosmic muons.

1.Introduction

An electromagnetic calorimeter based on liquid krypton (LKr) /1,2,5/ is developed for the KEDR detector /4/, which will be used at e^+e^- collider VEPP-4M with a beam energy of 5GeV. Use of liquid krypton in the calorimeter attractive due to the possibility to obtain good energy resolution (the same, as with NaI, CsI and BGO calorimeters) and better space resolution for photons in comparison with crystal calorimeters. This is due to the possibility of measuring a photon conversion point in cont-rast to the crystal detectors where the photon coordinates are determined by the shower center of gravity.

Moreover, longitudinal segmentation of LKr calorimeter provides important information for particle identification by dE/dx and also e/π -separation.

The amount of liquid krypton (35tons) necessary for the calorimeter can be quickly enough obtained, since krypton is industry produced and it is sufficiently pure, so that no further purification is needed.

2.The main properties of LKr

The main parameters of liquid krypton as a detector medium for calorimeter, compared to other materials, are presented in tables 1 and 2.

Krypton is radioactive due to the $\beta-$ decay of the ^{85}Kr isotope. The maximum electron energy is 0.67MeV, with an average energy of 0.25MeV and a half-life of 11yr. Our measurement of radioactivity with several samples of industrial krypton showed that 300 $\beta-$ decays/s occur in 1cm^3 of LKr in agreement with measurements performed by Lebedev and Bolozdynya (private communication).

Table 1
Properties of the materials for calorimeters.

	NaI	CsI	BGO	BaF	LAr	LKr	LXe
Density, g/cm^3	3.67	4.50	7.13	4.90	1.41	2.45	3.06
Rad.length, cm	2.59	1.85	1.12	2.10	13.5	4.60	2.80
Moliere rad., cm	4.31	3.76	2.70	–	10.0	6.66	5.71
Nucl. length, cm	41	84	22	30	84	60	55
(dE/dx)$_{min}$ MeV/cm	4.85	5.60	9.20	–	2.31	3.45	3.89
Rad. resistance	sat.	sat.	sat.	good	fine	fine	fine

Table 2
Physical properties of LAr, LKr and LXe.

	LAr	LKr	LXe
Atomic number Z	18	36	54
Atomic mass A	40	84	131
T (boiling at 1 atm), K	87.3	119.8	165.1
T (freezing at 1 atm), K	83.8	116.0	161.4
Liquid/gas density ratio	784	641	519
Ionization energy, eV/pair	24.4	20.5	15.6
e drift vel. at 1kV/cm, mm/s [a]	1.8	2.4	2.2

a) Data from Ref.3.

3. Space characteristics of showers in LKr

Using Monte-Carlo simulation, we have calculated main characteristics of showers produced by photons in LKr. A part of this calculations was made with the magnetic field of 1.8 Tesla directed perpendicularly to the shower axis.

In table 3 we present the average energy deposition W and fluctuations of the energy deposition σ_W/E in a LKr layer with a thickness of 70 cm ($15.1X_0$). The quantity σ_W is calculated as FWHM over 2.36.

Table 3
Energy deposition W/E and its fluctuations.

E, GeV	0.1	0.2	0.5	1	2	5
W/E ,%	98.6	98.4	98.0	97.3	96.0	95.2
σ_W/E, %	0.4	0.5	0.8	1.1	1.4	2.3

Data concerning energy fraction (K_B), going back from LKr, as a function of energy of photon, falling normally to the surface, are presented in table 4.

Table 4
Fraction of photon energy going back from LKr.

E, GeV		0.05	0.1	0.2	0.5	1	5
K_B, %	H=0	0.76	0.53	0.35	0.27	0.22	0.09
	H=18 T	1.2	0.87	0.61	0.43	0.33	0.18

The energy fraction of photon, deposited in a cylinder with a radius R and 70cm length is given in fig.1. Calculations were carried out for photons at 0.1 and 1GeV with and without magnetic field. One can see, that at H=1.8T the transverse size of shower icreased approximately in a factor of 1.2 at 90% level of absorbed energy.

In figs. 2 and 3 data are presented for the case, when a photon falls on the calorimeter at some distance from the boundary between two large blocks (H=0). The average energy leaking in the neighbouring block and the value of its fluctuationsare shown. The thickness of LKr is 70cm. The photon energies are 0.1 and 0.5GeV. These data are useful for the estimation of the energy resolution for events with two photons close in space. If, for example, photons have energy about 0.1GeV, their energy can be reconstructed with a 6% accuracy for a 8cm distance between the photons and 3% for a 16cm distance.
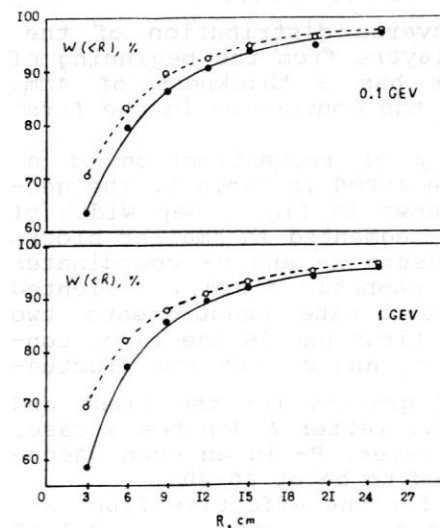

Fig.1. Fraction of the photon energy (%) deposited in a 70cm LKr cylinder versus its radius. Photon energy equals to 0.1 and 1GeV. The solid line is for H=1.8T, dashed line is for H=0.
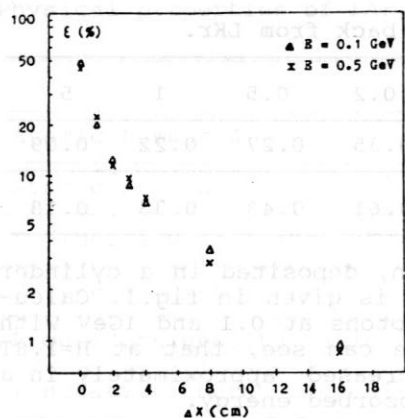
Fig.2. Fraction of the photon energy going to the neighboring block versus a distance from the photon to the boundary between blocks.
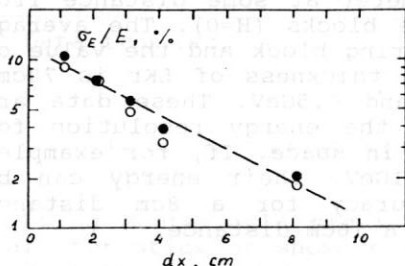

Fig.3. Fluctuation of the fraction of energy going to the neighboring block versus a distance from the photon to the boundary between blocks.

Figs. 4 and 5 depict transverse distribution of the shower energy in first three layers from the beginning of the shower (H=0). Each layer has a thickness of 4cm. Events have been selected with the conversion in the first layer.

The data concerning accuracy of reconstraction of a photon conversion point are presented in table 5. The geometry of the calorimeter is shown in fig.6. Gap width of LKr is $\Delta z=4$cm. This layers are segmented in smaller blocks in transverse direction to measure x- and y- coordinates (odd and even layers, resp.). Magnetic field is oriented in x- direction. For the coordinate measurements two neighbour layers are used. The first one is the layer containing the conversion point. σ_1 and σ_2 are rms fluctuations of the shower center of gravity for the first and the second layers, respectively. Letter A denotes a case, when conversion was in an odd layer, B- in an even. Accuracy of calculation is estimated to be of 10-20%.

In fig.7 data are presented for the effective fluctuation in a case with H=1.8T $\sigma=\frac{1}{2}[(\sigma_1^A)^2+(\sigma_2^A)^2+(\sigma_1^B)^2+(\sigma_2^B)^2]^{1/2}$ and with H=0 $\sigma=[(\sigma_1^2+\sigma_2^2)/2]^{1/2}$
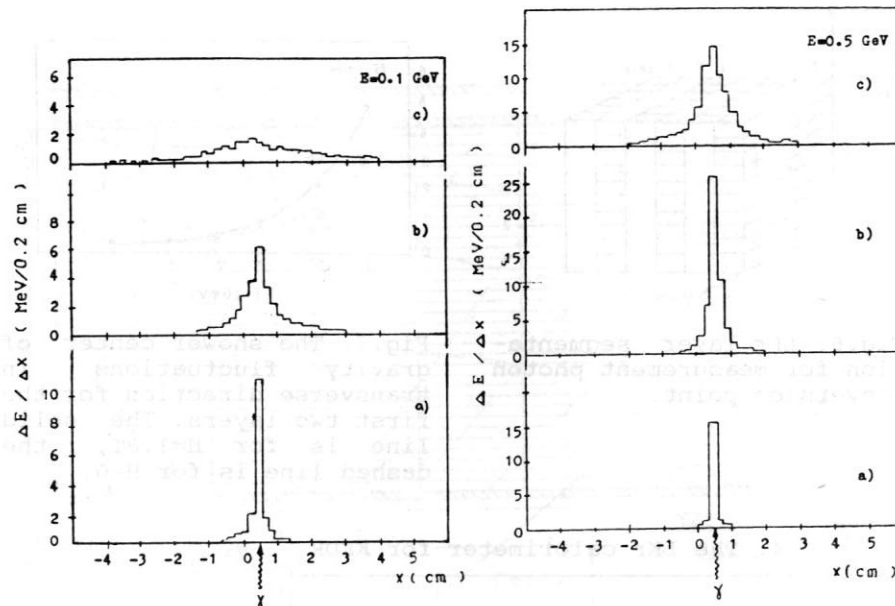

Fig.4. The transverse distribution of the energy released in the first layers for the photon energy of 0.1GeV. a) 1-st layer, b) 2-nd layer, c) 3-d layer. The layer thickness is 4cm.

Fig.5. The same as fig.4 for the photon energy of 0.5GeV.

Table 5
Fluctuations of the center of gravity σ(mm).

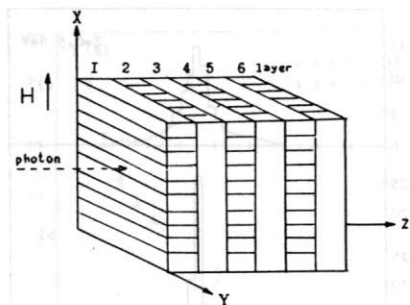| E	H=1.8T, case A		H=1.8T, case B		H=0	
(GeV)	σ_1^A	σ_2^A	σ_1^B	σ_2^B	σ_1	σ_2
0.1	0.55	8.5	0.55	4.0	0.5	4.0
0.2	0.35	3.6	0.35	2.0	0.3	1.6
0.5	0.22	1.3	0.24	1.0	0.17	1.0
1.0	0.12	0.7	0.14	0.55	0.13	0.5
2.0	0.10	0.35	0.10	0.35	0.06	0.35
5.0	0.06	0.30	0.09	0.30	0.06	0.30

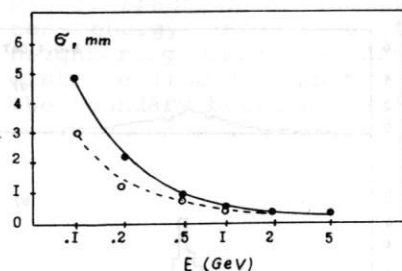Fig.6. LKr layer segmentation for measurement photon conversion point.

Fig.7. The shower center of gravity fluctuations in transverse direction for the first two layers. The solid line is for H=1.8T, the dashed line is for H=0.

4. The LKr calorimeter for KEDR

The e.m. calorimeter of KEDR consists of two types: the end-cap is made of CsI (3tons), barrel part is built of LKr. Construction of the LKr calorimeter is presented in figs 8 and 9. The outer diameter and the lenght are about 3m. The inner volume of the cryostat contains 35tons of LKr. Outer (warm) walls of the cryostate are made of stainless steel, inner (cold) are made of aluminum alloy. The cooling of the cryostat is realized by liquid nitrogen under the preasure of 20 atmospheres. The material thickness in front of LKr is 1mm of Fe and 14mm of Al. The electrodes thickness is 0.5mm of G10 and $2 \cdot 18 \mu m$ of Cu. A gap between electrodes is 2cm.

The signal read - out for the energy measurement is carried out from high voltage electrodes, divided into rectangular pads, forming towers, aimed at the interaction point. Towers entrance size is $10 \cdot 10 cm^2$. In radial direction all towers are divided into three layers. The grounded electrodes of the first layers of 30cm thickness are divided into strips of about 5mm width in the direction along the beam line (Z-axis) and in orthogonal one (ϕ). These strips are used for the measurement of the photon coordinates and for dE/dx. There are in total 8 strip layers. The width of the towers and Z-strips is increased along Z- axis to provide the uniform resolution in the polar angle.
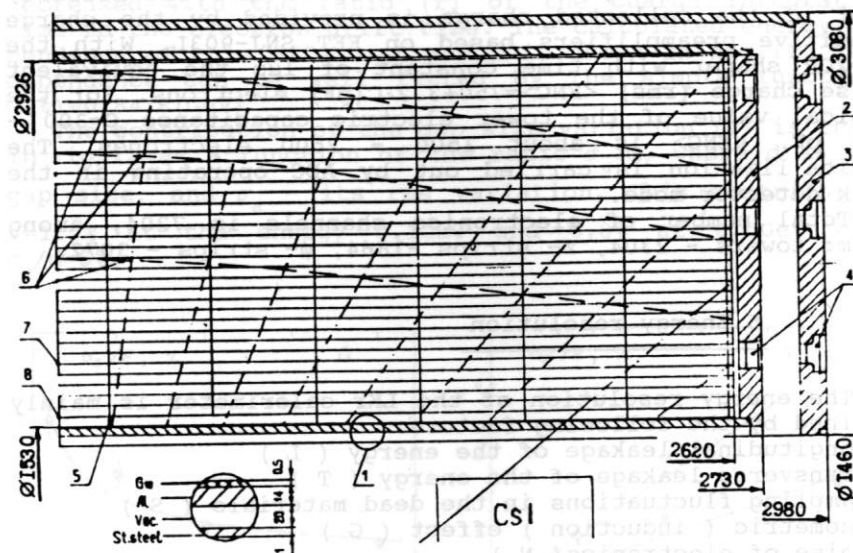
Fig.8 Layout of the LKr calorimeter. 1- entrance wall, 2- cold flange, 3-warm flange, 4- feedthroughs, 5- spacers, 6- lines of equal thickness, 7- strip electrode, 8- high voltage (tower) electrode.
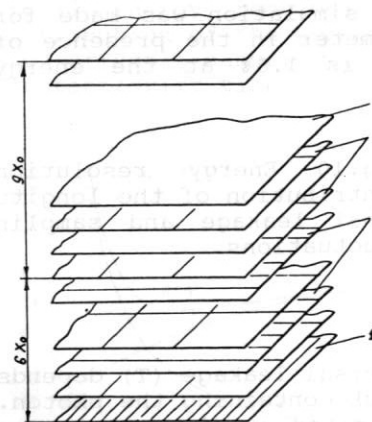

Fig.9 The scheme of the electrodes structure. 1- z-strips, 2- ϕ.strips, 3- towers, 4- grounded electrodes.

The ionization chambers of the calorimeter are operated in the electron - pulse mode. The electrons drift time at the electric voltage of 1kV is close to 8μs. The measurement of the collected charge is provided by the charge sensitive preamplifiers based on FET SNJ-903L. With the RC-2CR shaper with time constant of 1μs the equivalent noise charge (rms) <ENC>=750+3.2·C(pF) electrons. For the typical value of the tower electric capacitance C=300 - 500 pF, <ENC> is about 1500 - 2500 electrones. The digitalization is carried out by ADC operating in the peak detector mode.

Total number of electronics channels is 7204, among them: towers - 2304, z- strips -1864, φ- strips - 3072.

5.Energy resolution

The energy resolution of the LKr calorimeter is mainly defined by the following factors:
- Longitudinal leakage of the energy (L)
- Transverse leakage of the energy (T)
- Sampling fluctuations in the dead materials (S)
- Geometric (induction) effect (G)
- Noise of electronics(N)
- Radioactivity of LKr (R)
- Variation of the gaps (V)
- Calibration inaccuracy, electronics instability
- Algorithm of energy reconstruction

In fig.10 it is shown the result of Monte-Carlo computation of the contribution of the longitudinal leakage and sampling fluctuations (L+S). The simulation was made for the real structure of the calorimeter in the presence of the magnetic field. The result is 1.8% at the energy 0.1GeV and 1.1% at 0.5 GeV.
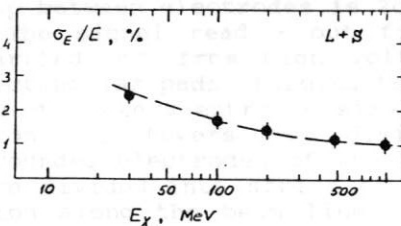
Fig.10 Energy resolution. Contribution of the longitudinal leakage and sampling fluctuations.

The contribution of the transversal leakage (T) depends on the acceptable size of the block containing the photon. For example, if this block is limited in the one transverse direction only and the distance to the flat bound is dx, the relative fluctuations of the leaked energy is shown in fig.3.

The geometric (induction) effect (G) arises from the

dependence of the collected charge on the ionization distribution inside the gap. The magnitude of this effect is decreased with the ratio (r) of the charge integration time to the electron drift time. The calculated energy dependence of this effect at r=0.1 is shown in fig.11. This dependence can be well fitted by the simple function:
$$G(\%)=0.84 \cdot E(GeV)^{-0.4}.$$

The contribution of the gap size variation (V) is shown in fig.12 as a function of the ratio σ_d/d, where d is the gap size, and σ_d - its rms variation. This contribution V=1.7% at the energy 0.1GeV and 0.8% at 0.5GeV when σ_d/d=5%.
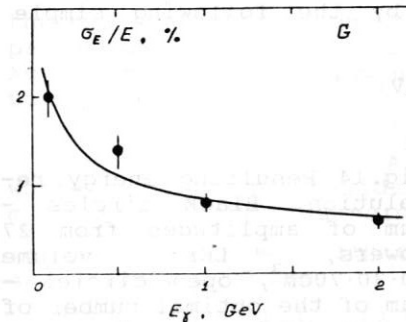
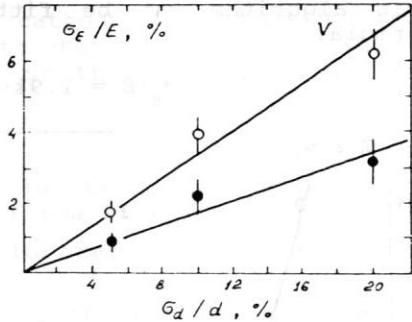Fig.11 Energy resolution. Contribution of the geometric effect; shaper time constant/drift time = 0.1.

Fig.12 Energy resolution. Contribution of the gap variance. Black circles is for E$_\gamma$=0.5GeV, open is for E$_\gamma$=0.1GeV.
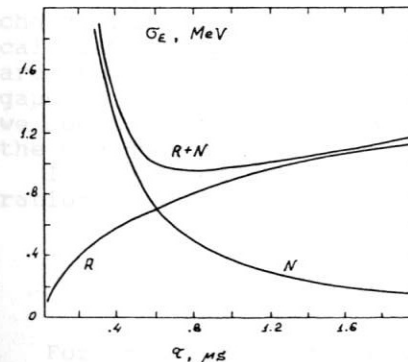
Fig.13 Energy resolution. Electronics and radioactive noise for 1 tower versus time constant.

The electronics noise has to be treated together with the LKr radioactiv noise. The electronics and radioactive noise contribution is shown in fig.13 versus time constant of the RC-2CR shaper. The calculation has been performed for the one block of the tower with the capacitance of 250pF and LKr volume of 5 liters. The equivalent noise of one block at the optimal time constant of $1\mu s$ equals 0.9MeV.

The calculation of the energy resolution taking into account all mentioned above effects is shown in fig.14 as a function of the photon energy. The results of using two various algorithms are presented: the first one- summing of amplitudes of 27 blocks (the full size is $30 \cdot 30 \cdot 70$ cm^3); another one- summing of optimal (for each energy) number of blocks from the same volume. The result of the this algorithm can be fitted by the following simple formula:
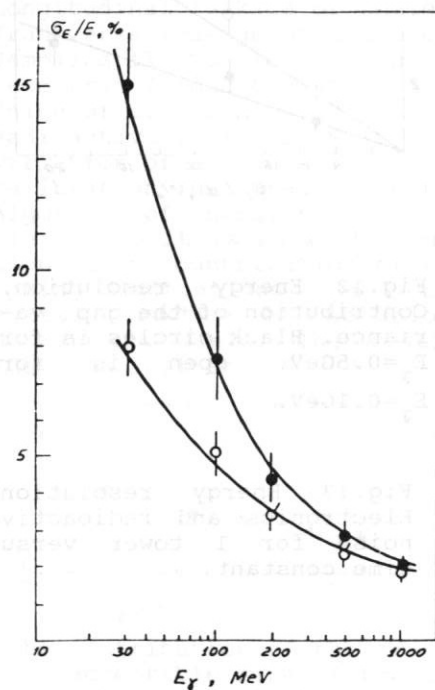
$$\sigma_E/E = 1.9\% \cdot E(GeV)^{-0.4}$$

Fig.14 Resulting energy resolution. Black circles - sum of amplitudes from 27 towers, LKr volume $30 \cdot 30 \cdot 70$cm^3, open circles - sum of the optimal number of towers amplitudes from the same volume.

6. Space resolution.

The space resolution for photons is determined by the

---

fluctuations of the shower gravity center and by the measurement precision of the ionization position. The fluctuation of the shower was discussed in the 3-rd section (table 5 and fig.7). Remark that the fluctuation value in the second layer depends on the layer thickness Δz as $\Delta z^{3/2}$.

The measurement precision of the ionization position has some pecularity which depends on many parameters /2/. Charge distribution on the anode is strongly peaked with opposite sign "tails". If a charge of one sign only is measured at the anode, the coordinate is determined by the strips width s, the corresponding accuracy is $\sigma_x = s/\sqrt{12}$.

In the case when the integration time τ_i is more than the total drift time of electrons in the gap T_d ($\tau_i > \bar{T}_d$), the charge distribution at the cathode is less peaked compared one at the anode and with "tails" of the same sign. As shown in /2/ the accuracy of the gravity center determination is

$$\sigma_x \sim s \cdot \frac{\sigma_n}{A}$$

where s is the strip width, A is the signal pulse hight, σ_n is the electronics noise. If the signal to noise ratio is 50 (what is easy achieved for relativistic particles) and s=10mm, $\sigma_x = 0.2$mm.

When only a small fraction of the charge is collected ($\tau_i \ll T_d$) the distribution of the charge on the cathode is very narrow and the resolution is about $s/\sqrt{12}$.

7. The particle identification.

Puls hight measurements from the strips can be used for charge particles identification by the dE/dx method. The calculation results for π-K separation with 5 gaps of LKr are shown in fig.15 together with dE/dx information in 42 gaps of the KEDR drift chamber (DME at 1 atmosphere). As we see LKr gives π-K separation at the level over 2σ up to the momentum 1GeV.

In fig.16 we show the calculation results for π-K separation if 150 gas gaps and 20 LKr gaps would be used.

8. The prototype test results

For the experimental study of the LKr technique we have built two prototypes: Prototype-7 (7kg of LKr) and Prototype-400 (400 of LKr). The first one was aimed at the
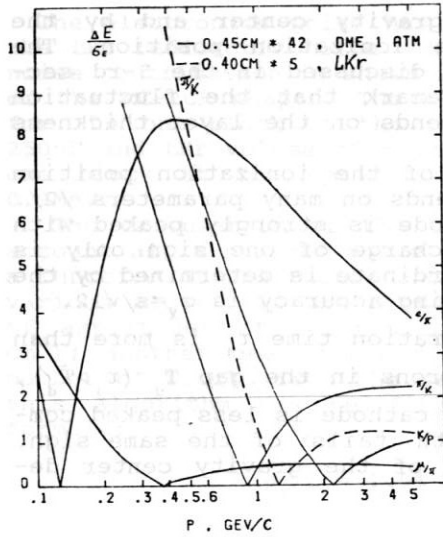
Fig.15 Particle identification by dE/dx. π-K separation: the solid line is for 42 gaps of the drift chamber, the dashed line is for 5 gaps of LKr.

Fig.16 The π-K separation by dE/dx. The dashed line is for 20 gaps of LKr. The dot and dash line is for 150 gaps of DME at 1 atm. The solid line is for using both.

measurement of the space resolution for the charged particles. It was consisted of four ionization chambers with the gap of 1cm thickness. The readout electrodes were divided into 5 strips each with a width of 1cm. Signal processing was carried out by charge sensitive preamplifiers, RC-CR shaper and peak ADC connected to each strip. The time constant of the shaper was 3μs, drift time about 4μs.

In the experiment with cosmic particles we obtained space resolution σ=3mm in anode readout mode and σ=0.4mm in cathode readout with center of gravity method. The result for cathode readout is shown in fig.17. The details of this experiment are described elsewhere /2/.

The experiment with Prototype-400 was devoted to the energy resolution measurement. The Prototype-400 lay-out is shown in fig.18. The electrode system was consisted of 19 flat ionization chambers with the 20mm gap. The thickness of electrodes was 0.5mm G10+2·35m of copper. Diameter of this calorimeter was 45cm, the length was 76cm. All odd electrodes were connected to charge sensitive pre-
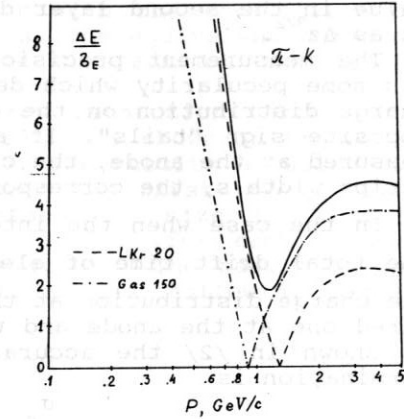
amplifiers based on FET SNJ-903L. Signal processing was carried out by RC-2CR shaper and peak ADC.
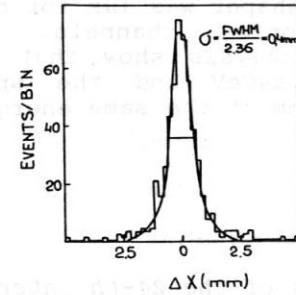

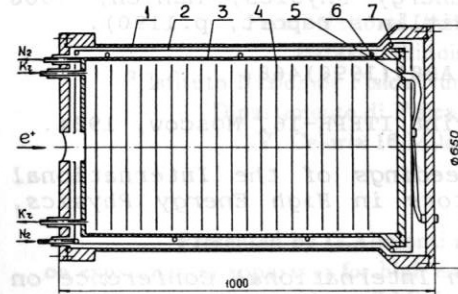Fig.17 Space resolution at cosmic particles.

Fig.18 Prototype-400, layout. 1- external volume, 2- liquid Nitrogen copper screen, 3- internal volume, 4- electrodes, 5- feed-through, 6,7- cooling pipes.

The experiment was performed with the positrons in the energy region from 0.13 to 1.2 GeV. The results of the experiment are shown in fig.19. For details see Ref.2. The obtained energy resolution is practically the same that was obtained in CLEO-2 and KEDR CsI calorimeter prototypes and in L3 BGO calorimeter prototype.
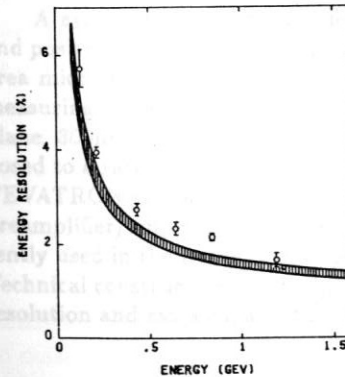

Fig.19 Energy resolution (rms) of 0.4 ton liquid krypton calorimeter (point); the band (±σ) shows the resalt of calculation including statistical errors of simulation and possible uncertainty of the electronic and radioactive noise.

During March - April 1990 we have performed a new experiment with Prototype-400. There was replaced electrode system to be close to the KEDR calorimeter electrode

structure, containing towers and strips, except the strip width, which was 10cm. It also included at the first time the read-out from both electrodes of the ionization chambers. The time constant of the shaper was $1\mu s$ for both the towers and strips electronics channels. The preliminary results of the data analysis show that the energy resolution is 2.3% at 0.84GeV and the space resolution for the first gap is 2.2mm at the same energy.

References

1. V.M.Aulchenko et al., *Proceedings of the 24-th International Conference on High Energy Physics*, Munich, 1988 (contributed paper N 833, D.Hitlin's report, p.1190).

2. V.M.Aulchenko et al., *NIM* A289(1990)468.

3. C.N.Anisimov et al., *Preprint* ITEPH-16, Moscow, 1984.

4. V.V.Anashin et al., *Proceedings of the International Simposium on Position Detectors in High Energy Physics*, Dubna, 1988, p.58.

5. V.M.Aulchenko et al., *5-th International Conference on Instrumentation for Colliding Beam Physics*, March 1990, Novosibirsk.

The wide band beam momentum tagging system at FNAL

G.Alimonti[1,2], J.Butler[1], W.R.Cavaletti[2], P.D'Angelo[2],

M.DiCorato[2], P.Inzani[2], S.Malvezzi[2], D.Menasce[2], L.Moroni[2],

D.Pedrini[2], F.Ragusa[2], S.Sala[2], M.Vittone[1]

[1] Fermi National Accelerator Laboratory
Batavia, Illinois 60510 -USA-
[2] Istituto Nazionale Fisica Nucleare - Sezione di Milano and
Dipartimento di Fisica- Universitá di Milano
V. Celoria 16 Milano 20134 -Milano-

Presented by G.Alimonti at the 4th topical seminar
on experimental apparatus for high energy particle physics and astrophysics
-S.Miniato, 1990-

ABSTRACT

A system to tag the particle momentum of the wide band primary electrons and positrons beam (PB EAST of FNAL) has been realized. It consists of five large area microstrip detectors, assembled in a symmetric two lever arm configuration, measuring the particle bend angles across the last pair of beam dipoles. Each silicon plane, $300\mu m$ thickness, consists of 256 microstrips with $300\mu m$ pitch and it is exposed to a rate of about 10^7 particles per sec. The system is capable to work at the TEVATRON radiofrequency (53 MHz). The readout electronics consists of a fast preamplifier/amplifier, a discriminator and a fast ecl memory. The system is currently used in the heavy quarks photoproduction experiment E687 at FERMILAB. Technical construction details, performances of the system (efficiencies, momentum resolution and rates capabilities) are presented.